AIMS Mathematics, 11(3): 6622–6648.
DOI: 10.3934/math.2026274
Received: 27 October 2025
Revised: 14 January 2026
Accepted: 20 January 2026
Published: 16 March 2026

https://www.aimspress.com/journal/Math

Research article

A comprehensive study of solitons and chaotic dynamics in the (3+1)-dimensional extended Kadomtsev-Petviashvili equation

Bahadır Kopçasız[1,*], Rubayyi T. Alqahtani[2] and Mehmet Şenol[3]

[1] Department of Mathematics, Kayseri Erciyes University, Melikgazi 38030, Türkiye

[2] Department of Mathematics and Statistics, College of Science, Imam Mohammad Ibn Saud Islamic University (IMSIU), Riyadh, Saudi Arabia; rtalqahtani@imamu.edu.sa

[3] Department of Mathematics, Nevşehir Hacı Bektaş Veli University, Nevşehir, Türkiye; msenol@nevsehir.edu.tr

* **Correspondence:** Email: bahadirkopcasiz@erciyes.edu.tr.

Abstract: This paper studies the analytical and dynamical behavior of a generalized (3+1)-dimensional extended Kadomtsev-Petviashvili (eKP) equation, which includes higher-order nonlinear and dispersive effects. Using the $\exp(-\varphi(\xi))$-expansion method, exact traveling wave solutions are obtained successfully. The solutions exhibit rich nonlinear wave structures, including localized solitons, periodic waves, and breathing patterns. To further explore the qualitative behavior of the system, a reduction of traveling waves is used, resulting in a planar dynamical system. A bifurcation analysis is carried out in detail by investigating the equilibrium points, Jacobian structures, and their relations to system parameters. The phase portraits show topological transitions such as centers, saddles, and cusp points. Moreover, a perturbed form of the reduced system is considered in order to investigate chaotic dynamics under periodic external forcing. The existence of chaos is verified using bifurcation diagrams, sensitivity analysis, Poincaré maps, time series, and both 2D and 3D phase portraits. These numerical simulations confirm the theoretical predictions and demonstrate the system's complex behavior across varying perturbation parameters. Overall, the outcomes provide a complete picture of the soliton structures and chaotic regimes that the eKP model may exhibit in physico-nonlinear wave propagation in multidimensional contexts.

Keywords: bifurcation analysis; chaotic dynamics; extended Kadomtsev-Petviashvili equation; soliton solutions; $\exp(-\varphi(\xi))$-expansion method
Mathematics Subject Classification: 35C07, 37D45, 37G15, 35Q53

1. Introduction

Partial differential equations (PDEs) are one of the most fundamental mathematical systems for describing the spatial and temporal behavior of an extensive range of physical phenomena, including heat conduction, fluid flows, electromagnetic wave propagation, and wave dynamics. Although linear PDEs have been extensively investigated and possess well-developed analytical and numerical methods of solution, their nonlinear counterparts-nonlinear partial differential equations (NLPDEs)-pose astronomically larger mathematical and computational challenges. Nonlinearity occurs when the dependent variable or its derivatives are involved in a nonlinear fashion, for instance, through nonlinear terms, products of derivatives, or nonlinear functional dependencies. This inherent complexity typically rules out the existence of general methods of solution and requires the creation of special analytical techniques or advanced numerical methods. In spite of their challenging nature, NLPDEs are unavoidable in providing an accurate description of real-world systems for which linearized approximations are incapable of capturing critical nonlinear interactions [1, 2].

NLPDEs typically do not have closed-form solutions and require advanced mathematical and computational methods, in contrast to linear PDEs, which typically allow the superposition of solutions and can be solved analytically by methods such as separation of variables or Fourier transforms. Many areas of science and engineering work with NLPDEs. Viscous fluid flow in fluid dynamics is controlled by the Navier-Stokes equations, which are nonlinear in nature. In general relativity, the curvature of spacetime is characterized by Einstein's field equations, which are NLPDEs. Nonlinear wave equations model a broad spectrum of phenomena, ranging from shallow water waves (by the Korteweg-de Vries (KdV) equation) to optical pulses in fiber optics (through the nonlinear Schrödinger equation) [3, 4]. Recent studies have further explored localized wave structures in extended Boussinesq-type (BO-type) systems, such as the dark localized waves reported by Yang et al. [5].

The Kadomtsev-Petviashvili (KP) hierarchy is a very notable paper in solitary waves theory that explains exciting higher-dimensional wave phenomena in NLPDEs. The KP hierarchy has some remarkable scientific properties and applications. Various extended KP hierarchies that keep the integrable structures of the original KP hierarchy have been constructed and thoroughly investigated in the literature.

Many studies on the KP Eq (1.1) and BO Eq (1.2) that exist in (1+1) dimensions and more than two dimensions have been studied exhaustively. In order to examine the stability of the well-known KdV equation in two-dimensional media, the traditional KP equation (1.1) was formulated. An ample amount of research has been carried out on the KP equation, which explains a broad variety of physical phenomena, such as fluid dynamics [6–8], dust acoustic waves, weakly nonlinear quasi-unidirectional waves [9–11], and many others. There exist families of exact solutions with novel characteristics for the KP equation. In addition to constant-coefficient KP models, variable-coefficient versions have also been extensively studied, yielding richer dynamical structures and more general wave behaviors; see, for example, Liu et al. [12], who developed a symbolic computation approach for multiple rogue wave solutions in variable-coefficient nonlinear systems.

The $\exp(-\varphi(\xi))$-expansion method is employed to systematically obtain many exact wave solutions. They include lump-wave and N-soliton solutions.

The following is the standard integrable KP equation [13]:

$$(\Gamma_t + 6\Gamma\Gamma_x + \Gamma_{xxx})_x + \lambda_0\Gamma_{yy} = 0. \tag{1.1}$$

It has a weak dispersion term (Γ_{xxxx}) and a quadratic nonlinearity term $(\Gamma\Gamma_x)_x$, admitting weakly dispersive waves. Equation (1.1) is used in many physical contexts and describes the phenomenon of small surface tension relative to the gravitational force in fluid dynamics [14–16]. However, the BO equation says

$$\Gamma_{tt} - \Gamma_{xxxx} - \Gamma_{xx} - 3(\Gamma^2)_{xx} = 0, \tag{1.2}$$

where the height of a fluid's free surface is represented by the real-valued, sufficiently often differentiable function $\Gamma(x,t)$, and partial derivatives are indicated by subscripts. Small-amplitude dispersive waves traveling in both left and right directions in shallow water are modeled by the BO Eq (1.2) [17–20]. A great deal of research has been done to investigate a large number of exact solutions to the two well-known Eqs (1.1) and (1.2).

Additionally, the following extended Kadomtsev-Petviashvili (eKP) equation was proposed in [21]:

$$(\Gamma_t + 6\Gamma\Gamma_x + \Gamma_{xxx})_x - \Gamma_{yy} + \lambda_0\Gamma_{tt} + \mu\Gamma_{yt} = 0, \tag{1.3}$$

where

$$\Gamma = \Gamma(x,y,t)$$

is a differentiable function, λ_0 and μ are non-zero constants, and $\lambda_0\Gamma_{tt}$ and $\mu\Gamma_{yt}$ are added to the standard KP Eq (1.1). The KP equation can also be extended as follows [22]:

$$(\Gamma_t + 6\Gamma\Gamma_x + \Gamma_{xxx})_x - \Gamma_{yy} + \frac{\alpha^2}{4}\Gamma_{tt} + \alpha\Gamma_{yt} + \beta\Gamma_{xt} = 0. \tag{1.4}$$

Finally, three (2+1)-dimensional dispersive equations are presented in [23] as

$$\Gamma_{xt} + \alpha(\Gamma_{xxxx} + 6\Gamma_x\Gamma_{xx}) + \beta\Gamma_{yy} + a\Gamma_{xx} + b\Gamma_{xy} = 0, \tag{1.5}$$

$$\Gamma_{xt} + \alpha(\Gamma_{xxxx} + 6\Gamma_x\Gamma_{xx}) + \beta\Gamma_{tt} + a\Gamma_{xx} + b\Gamma_{xy} = 0, \tag{1.6}$$

and

$$\Gamma_{xt} + \alpha(\Gamma_{xxxx} + 6\Gamma_x\Gamma_{xx}) + \beta\Gamma_{yy} + \gamma\Gamma_{tt} + a\Gamma_{xx} + b\Gamma_{xy} + c\Gamma_{yt} = 0, \tag{1.7}$$

where $\alpha, \beta, \gamma, a, b$, and c are arbitrary parameters, and

$$\Gamma = \Gamma(x,y,t)$$

is a differentiable function with respect to the spatial variables x and y and the temporal variable t.

Three new (3+1)-dimensional equations have been proposed very recently in [24],

$$(\Gamma_t + 6\Gamma\Gamma_x + \Gamma_{xxx})_x + \lambda_1\Gamma_{xx} + \lambda_2\Gamma_{xy} + \lambda_3\Gamma_{xz} + \alpha\Gamma_{yy} = 0, \tag{1.8}$$

$$(\Gamma_t + 6\Gamma\Gamma_x + \Gamma_{xxx})_x + \lambda_1\Gamma_{xx} + \lambda_2\Gamma_{xy} + \lambda_3\Gamma_{xz} + \beta\Gamma_{zz} = 0, \tag{1.9}$$

$$(\Gamma_t + 6\Gamma\Gamma_x + \Gamma_{xxx})_x + \lambda_1\Gamma_{xx} + \lambda_2\Gamma_{xy} + \lambda_3\Gamma_{xz} + \gamma\Gamma_{tt} = 0, \tag{1.10}$$

which will be called the first eKP (1eKP) equation, second eKP (2eKP) equation, and eKP-Boussinesq (eKP-BO) equation, respectively, where α, β, γ, and λ_i (i = 1,2,3) are nonzero parameters. Notice that

the last term in each equation of (1.8)–(1.10) is the only term that changes between these equations, whereas the other terms in each equation remain unchanged. It is worth noting that the integrability of these equations was already verified in the seminal work of Wazwaz [24], where a detailed Painlevé analysis confirmed that the models possess the Painlevé property.

This study concentrates on the (3 + 1)-dimensional 1eKP Eq (1.8), where α and λ_i ($i = 1, 2, 3$) are nonzero arbitrary parameters, and

$$\Gamma = \Gamma(x, y, z, t)$$

is a differentiable function involving the spatial variables x, y, and z, and the temporal variable t. It is clear that the terms $\alpha\Gamma_{yy}$ in Eq (1.8) and $\beta\Gamma_{zz}$ in Eq (1.9), respectively, are replaced by the term $\gamma\Gamma_{tt}$ in Eq (1.10). The conventional Boussinesq equation typically contains the terms $\gamma\Gamma_{tt}$, Γ_{xxxx}, and $\lambda_1\Gamma_{xx}$ in Eq (1.10).

We derive several soliton solutions to illustrate the wealth of analytical structure of the 1eKP equation. Furthermore, a class of lump-type solutions is investigated for different parameter regimes, illustrating the variety and flexibility of exact wave structures supported by the model. Such results not only enhance the insight into the underlying nonlinear dynamics but also provide useful benchmarks for the validation of numerical algorithms. Due to their complexity and applicability, such equations are routinely employed in computational mathematics for testing, calibrating, and verifying methods for NLPDEs, with implications for both theoretical development and applied modeling.

To analyze the nonlinear structure of the eKP equation, the remainder of the manuscript is organized into several interconnected components. First, in Section 2, the $\exp(-\varphi(\xi))$-expansion method is introduced, and in Section 3, it is applied to derive explicit traveling-wave solutions. Section 4 provides graphical visualizations of these solutions, highlighting their solitonic, oscillatory, and structural features. Then, a traveling-wave reduction is employed to obtain a planar dynamical system, whose qualitative behavior, equilibrium properties, and bifurcation mechanisms are analyzed in Section 5. Section 6 then investigates the chaotic dynamics arising from periodic perturbations of the reduced system through bifurcation diagrams, sensitivity analysis, phase portraits, Poincaré sections, and time-series simulations. Finally, Section 7 summarizes the numerical findings and discusses their consistency with the analytical results. Together, these components provide a coherent analytical and numerical framework for understanding the rich wave phenomena captured by the extended KP equation.

2. The $\exp(-\varphi(\xi))$-expansion method

This method is particularly effective for nonlinear dispersive equations because it converts the PDE into an ordinary differential equation (ODE) with a closed-form auxiliary equation, allowing construction of soliton and periodic wave solutions.

Examine the nonlinear equation, which is presented as follows:

$$\mathscr{P}(\Gamma, \Gamma_x, \Gamma_y, \Gamma_z, \Gamma_t, \Gamma_{xx}, \Gamma_{xy}, \Gamma_{xz}, \ldots) = 0. \tag{2.1}$$

When $\mathscr{P}$ is a polynomial of $\Gamma(x, y, z, t)$ and its derivatives, the subscripts signify partial derivatives. During utilizing the $\exp(-\varphi(\xi))$-expansion method [25] for obtaining wave solutions of Eq (2.1), it is crucial to carry out the following procedures.

- The real variables (x, y, z, t) are combined using ξ as a compound variable.

$$\xi = ax + by + cz + dt, \quad \Gamma(x, y, z, t) = \psi(\xi). \tag{2.2}$$

To ensure that the transformation involves all four independent variables, x, y, z, and t and to avoid degeneracies in the solution process, we assume that $a \neq 0$, $b \neq 0$, $c \neq 0$, and $d \neq 0$.

- Equation (2.1) is reduced to yield the following ODE:

$$\mathscr{H}(\psi(\xi), \psi'(\xi), \psi''(\xi), \ldots) = 0. \tag{2.3}$$

- The following finite series can be used to construct the precise solutions

$$\psi(\xi) = \sum_{r=0}^{N} B_r (exp(-\varphi(\xi)))^r, \quad B_N \neq 0, \quad 0 \leq r \leq N. \tag{2.4}$$

- The following ODE is satisfied by $\varphi = \varphi(\xi)$:

$$\varphi'(\xi) = exp(-\varphi(\xi)) + \eta\, exp(\varphi(\xi)) + \lambda. \tag{2.5}$$

- Equation (2.5) yields the following solutions when $\eta \neq 0$ and $\lambda^2 - 4\eta > 0$, depending on certain parameters:

$$\psi_1(\xi) = \frac{\ln\left(-\sqrt{(\lambda^2 - 4\eta)}\tanh\left(\frac{\sqrt{(\lambda^2-4\eta)}}{2}(h + \xi)\right) - \lambda\right)}{2\eta} \tag{2.6}$$

in the case of $\eta \neq 0$ and $\lambda^2 - 4\eta < 0$,

$$\psi_2(\xi) = \frac{\ln\left(\sqrt{(4\eta - \lambda^2)}\tanh\left(\frac{\sqrt{(4\eta-\lambda^2)}}{2}(h + \xi)\right) - \lambda\right)}{2\eta} \tag{2.7}$$

in the case of $\eta = 0$, $\lambda \neq 0$ and $\lambda^2 - 4\eta > 0$,

$$\psi_3(\xi) = -\ln\left(\frac{\lambda}{\sinh(\lambda(h + \xi)) + \cosh(\lambda(h + \xi)) - 1}\right) \tag{2.8}$$

in the case of $\eta \neq 0$, $\lambda \neq 0$ and $\lambda^2 - 4\eta = 0$,

$$\psi_4(\xi) = \ln\left(-\frac{2(\lambda(h + \xi) + 2)}{\lambda^2(h + \xi)}\right) \tag{2.9}$$

in the case of $\eta = 0$, $\lambda = 0$ and $\lambda^2 - 4\eta = 0$,

$$\psi_5(\xi) = \ln(h + \xi), \tag{2.10}$$

where the constant for integration is h.

- The determination of the N value in Eq (2.4) involves considering the balance principle among the highest-order derivatives and the highest-order nonlinear terms of $\psi(\xi)$ in Eq (2.3). When Eq (2.4) is combined with Eqs (2.3) and (2.5) with terms having the same $\exp(-\varphi(\xi))$ powers, the left-hand side of Eq (2.5) transforms into a polynomial. This transformation results in a system of algebraic equations involving the variables B_r $(r = 0, 1, 2, 3, \ldots, N)$, h, λ, and η. Solving Eq (2.5) by setting all coefficients of this polynomial to zero, we obtain a system of algebraic equations involving the parameters B_r, h, λ, and η.

3. Analytical solutions by the exp$(-\varphi(\xi))$-expansion method

After applying the transformation, the reduced ODE allows us to identify the balance between the nonlinear and dispersive terms and determine the structure of admissible exact solutions.

Let us consider Eq (1.8). After using Eq (2.2), integrals are taken for ξ, and the following ODE is obtained:

$$\left(a^2\lambda_1 + ab\lambda_2 + ac\lambda_3 + ad + \alpha b^2\right)\psi(\xi) + 3a^2\psi(\xi)^2 + a^4\psi''(\xi) = 0. \tag{3.1}$$

If a balancing relationship is established between ψ^2 and ψ'', the balancing constant $N = 2$ is found. From Eq (2.5), we have

$$\psi = a_0 + a_1\exp(-\varphi(\xi)) + a_2\exp(-\varphi(\xi))^2. \tag{3.2}$$

When the steps of the offered method are followed, the next system of algebraic equations is obtained:

$$\begin{aligned}
0 &= a_1a^4\lambda\eta + 2a_2a^4\eta^2 + a_0a^2\lambda_1 + 3a_0^2a^2 + \alpha a_0b^2 + a_0ab\lambda_2 + a_0ac\lambda_3 + a_0ad,\\
0 &= 6a_2a^4 + 3a_2^2a^2,\\
0 &= 10a_2a^4\lambda + 2a_1a^4 + 6a_1a_2a^2,\\
0 &= 4a_2a^4\lambda^2 + 3a_1a^4\lambda + 8a_2a^4\eta + a_2a^2\lambda_1 + 3a_1^2a^2 + 6a_0a_2a^2 + \alpha a_2b^2 + a_2ac\lambda_3 + a_2ad + aa_2b\lambda_2,\\
0 &= a_1a^4\lambda^2 + 6a_2a^4\lambda\eta + 2a_1a^4\eta + a_1a^2\lambda_1 + 6a_0a_1a^2 + \alpha a_1b^2 + a_1ab\lambda_2 + a_1ac\lambda_3 + a_1ad.
\end{aligned}$$

After solving this system of algebraic equations, the following values are reached:

$$a_0 = -2a^2\eta,\quad a_1 = -2a^2\lambda\,,\quad a_2 = -2a^2,\quad d = -\frac{a^4\left(\lambda^2 - 4\eta\right) + a\left(a\lambda_1 + b\lambda_2 + c\lambda_3\right) + \alpha b^2}{a}.$$

In this case, the following results are obtained for solutions Eqs (2.6) and (2.10):

When $\lambda^2 - 4\eta > 0$, and $\eta \neq 0$, then

$$\begin{aligned}
\psi_1(x,y,z,t) = -2a^2\eta &- \frac{8a^2\eta^2}{\left(-\sqrt{\lambda^2-4\eta}\tanh\left(\frac{1}{2}\sqrt{\lambda^2-4\eta}\left(-\frac{t\left(a^4\left(\lambda^2-4\eta\right)+a\left(a\lambda_1+b\lambda_2+c\lambda_3\right)+\alpha b^2\right)}{a}+ax+by+cz+h\right)\right)-\lambda\right)^2}\\
&- \frac{4a^2\lambda\eta}{-\sqrt{\lambda^2-4\eta}\tanh\left(\frac{1}{2}\sqrt{\lambda^2-4\eta}\left(-\frac{t\left(a^4\left(\lambda^2-4\eta\right)+a\left(a\lambda_1+b\lambda_2+c\lambda_3\right)+\alpha b^2\right)}{a}+ax+by+cz+h\right)\right)-\lambda}.
\end{aligned} \tag{3.3}$$

When $\lambda^2 - 4\eta < 0$, and $\eta \neq 0$, then

$$\begin{aligned}
\psi_2(x,y,z,t) = -2a^2\eta &- \frac{8a^2\eta^2}{\left(\sqrt{4\eta-\lambda^2}\tan\left(\frac{1}{2}\sqrt{4\eta-\lambda^2}\left(-\frac{t\left(a^4\left(\lambda^2-4\eta\right)+a\left(a\lambda_1+b\lambda_2+c\lambda_3\right)+\alpha b^2\right)}{a}+ax+by+cz+h\right)\right)-\lambda\right)^2}\\
&- \frac{4a^2\lambda\eta}{\sqrt{4\eta-\lambda^2}\tan\left(\frac{1}{2}\sqrt{4\eta-\lambda^2}\left(-\frac{t\left(a^4\left(\lambda^2-4\eta\right)+a\left(a\lambda_1+b\lambda_2+c\lambda_3\right)+\alpha b^2\right)}{a}+ax+by+cz+h\right)\right)-\lambda}.
\end{aligned} \tag{3.4}$$

When $\lambda^2 - 4\eta > 0$, $\lambda \neq 0$, and $\eta = 0$, then

$$\begin{aligned}\psi_3(x,y,z,t) = &-\frac{2a^2\lambda^2}{\sinh(\lambda(ax+by+cz-\tau+h))+\cosh(\lambda(ax+by+cz-\tau+h))-1}\\ &-\frac{2a^2\lambda^2}{(\sinh(\lambda(ax+by+cz-\tau+h))+\cosh(\lambda(ax+by+cz-\tau+h))-1)^2},\end{aligned} \tag{3.5}$$

where

$$\tau = \frac{t\left(a^4\lambda^2 + a\left(a\lambda_1 + b\lambda_2 + c\lambda_3\right) + \alpha b^2\right)}{a}.$$

When $\lambda^2 - 4\eta = 0$, $\lambda \neq 0$, and $\eta \neq 0$, then

$$\begin{aligned}\psi_4(x,y,z,t) = &-\frac{a^2\lambda^4\left(-\frac{t\left(a(a\lambda_1+b\lambda_2+c\lambda_3)+\alpha b^2\right)}{a}+ax+by+cz+h\right)^2}{2\left(\lambda\left(-\frac{t\left(a(a\lambda_1+b\lambda_2+c\lambda_3)+\alpha b^2\right)}{a}+ax+by+cz+h\right)+2\right)^2}\\ &+\frac{a^2\lambda^3\left(-\frac{t\left(a(a\lambda_1+b\lambda_2+c\lambda_3)+\alpha b^2\right)}{a}+ax+by+cz+h\right)}{\lambda\left(-\frac{t\left(a(a\lambda_1+b\lambda_2+c\lambda_3)+\alpha b^2\right)}{a}+ax+by+cz+h\right)+2}-2a^2\eta.\end{aligned} \tag{3.6}$$

When $\lambda^2 - 4\eta = 0$, $\lambda = 0$, and $\eta = 0$, then

$$\begin{aligned}\psi_5(x,y,z,t) = \;&-2a^2\eta-\frac{2a^2\lambda}{-\frac{t\left(a^4\left(\lambda^2-4\eta\right)+a(a\lambda_1+b\lambda_2+c\lambda_3)+\alpha b^2\right)}{a}+ax+by+cz+h}\\ &-\frac{2a^2}{\left(-\frac{t\left(a^4\left(\lambda^2-4\eta\right)+a(a\lambda_1+b\lambda_2+c\lambda_3)+\alpha b^2\right)}{a}+ax+by+cz+h\right)^2},\end{aligned} \tag{3.7}$$

where h is the integration constant.

4. Visualization and interpretation of soliton structures

To illustrate the shapes and dynamical features of the analytical solutions, representative plots are provided for the cases corresponding to ψ_1, ψ_2, and ψ_3. The 3D soliton profile, contour plot, and 2D projection on a temporal slice in each plot reveal the wave structures' evolution and dynamics entirely. The graphical illustrations help clarify the physical shape and propagation characteristics of the analytical solutions derived in the previous section.

4.1. Soliton profile of ψ_1

Figure 1 displays the spatio-temporal dynamics of the soliton solution ψ_1 derived from Eq (3.3) for the condition $\lambda^2 - 4\eta > 0$ and $\eta \neq 0$. In panel (a), it is evident that the 3D surface plot represents a localized solitary wave preserving its form over propagation, thus verifying stability of the solution profile within the time interval considered. The panel (b) contour plot captures the symmetry and slope of the soliton, and panel (c) is a 2D projection at a specified temporal slice that highlights its

bell-shaped nature. The amplitude and width invariance with time signals the non-dispersive nature of the wave, a salient aspect of solitonic behavior.

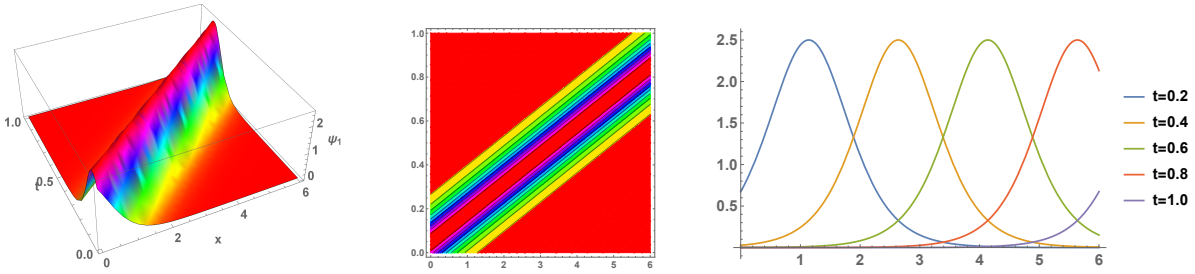

(a) **(b)** **(c)**

Figure 1. (a) The 3D soliton, (b) contour, and (c) 2D plot of ψ_1 appearing in equation (3.3) using the values $a = 1$, $b = 1$, $c = -2$, $\alpha = -1$, $\lambda = 3$, $\eta = 1$, $h = 0.5$, $\lambda_1 = 2$, $\lambda_2 = 0.7$, $\lambda_3 = -0.4$, $y = 1$, $z = 1$.

4.2. Breather-type profile of ψ_2

Figure 2 presents the breather-type profile ψ_2 corresponding to Eq (3.4) for the parameter regime $\lambda^2 - 4\eta < 0$ and $\eta \neq 0$. In this case, the solution exhibits a periodic-type oscillatory wave modulated in space and time, as shown in the 3D surface plot in panel (a). The contour plot in panel (b) illustrates the periodic peaks and valleys in the propagation direction, and the 2D projection in panel (c) illustrates the temporal periodicity and amplitude modulation. Its oscillatory character indicates the presence of wave trains rather than single pulses, and the shape is maintained by the competition between nonlinearity and dispersion in the system.

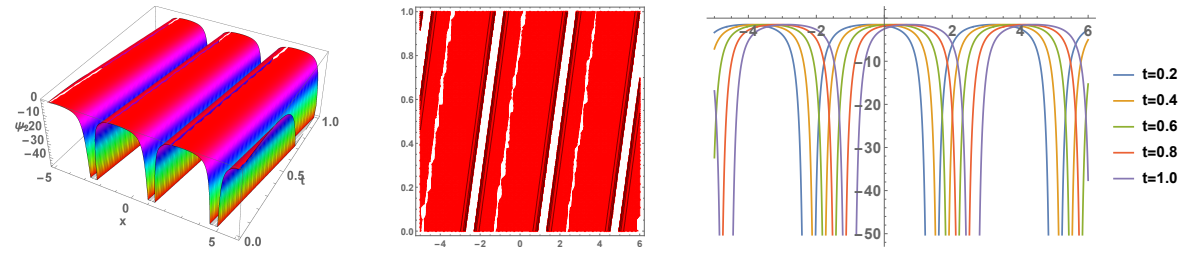

(a) **(b)** **(c)**

Figure 2. (a) The 3D breather solution, (b) contour, and (c) 2D plot of ψ_2 appearing in equation (3.4) using the values $a = 1$, $b = 1$, $c = -2$, $\alpha = 1$, $\lambda = 1$, $\eta = 1$, $h = 0.5$, $\lambda_1 = 2$, $\lambda_2 = 0.7$, $\lambda_3 = -0.4$, $y = 1$, $z = 1$.

A comparison between Figures 1 and 2 highlights the importance of the discriminant $\lambda^2 - 4\eta$ in deciding on the qualitative nature of the wave solutions. For $\lambda^2 - 4\eta > 0$, the model supports stable solitary pulses traveling undistorted, as shown in Figure 1. These localized profiles typify classical solitons resulting from an exact balance between nonlinear steepening and dispersive spreading. Yet, when $\lambda^2 - 4\eta < 0$, the solution turns into an oscillatory wave train, as depicted in Figure 2, with repetitive crests and troughs dominating the profile. This regime change from localized to periodic

solutions is a manifestation of the wave profile's sensitivity to changes in parameters and reflects the rich solution space of the eKP system.

It should be noted that the profile ψ_2 in Eq (3.4) contains a trigonometric term tan(·); therefore, it may exhibit singular spikes (vertical asymptotes) at discrete phase locations where the argument satisfies

$$\Theta(\xi) = \frac{\pi}{2} + k\pi, \quad k \in \mathbb{Z},$$

equivalently

$$\cos(\Theta(\xi)) = 0.$$

Thus, Eq (3.4) represents a periodic wave train that is smooth and bounded on intervals avoiding these poles, and becomes unbounded at the pole set. In the plotted parameter window of Figure 2, the spatio-temporal domain is chosen so that the solution is sampled away from the pole locations, yielding a regular oscillatory structure.

Apart from its soliton behavior, the (3+1)-dimensional 1eKP equation further possesses richer complex dynamical phenomena when studied through a reduced system. In the following section, the qualitative dynamics and bifurcation characteristics of the system are explored through tools of nonlinear dynamics.

5. Bifurcation analysis of the reduced dynamical system

This section examines how the reduced system behaves under parameter variations, allowing us to classify equilibrium points and understand transitions between different dynamical regimes.

5.1. Derivation of the reduced system

Bifurcation analysis aids in determining whether or not the underlying dynamical system depends on the values of the involved parameters. The Galilean transformation applied to Eq (3.1) yields the following planar dynamical system:

$$\begin{cases} \dfrac{d\psi}{d\xi} = \Omega, \\ \dfrac{d\Omega}{d\xi} = w_1\psi + w_2\psi^2, \end{cases} \tag{5.1}$$

where

$$w_1 = -\frac{a^2\lambda_1 + ab\lambda_2 + ac\lambda_3 + ad + \alpha b^2}{a^4} \quad \text{and} \quad w_2 = -\frac{3}{a^2}.$$

The Hamiltonian is given by

$$S(\psi, \Omega) = \frac{\Omega^2}{2} + w_1\frac{\psi^2}{2} + w_2\frac{\psi^3}{3} = s, \tag{5.2}$$

where the Hamiltonian constant is denoted by s. The bifurcations of the system (5.1) phase portraits throughout the parameter space of w_1 and w_2 will now be investigated. The following results can be seen through qualitative analysis.

5.2. Equilibrium points and Jacobian analysis

The first thing to note is that system (5.1) has two equilibrium points, which are as follows:

$$\mathcal{G}_1 = (0, 0) \quad \text{and} \quad \mathcal{G}_2 = \left(\frac{-w_1}{w_2}, 0\right).$$

The Jacobian of (5.1) will be

$$J(\psi, \Omega) = \det \begin{vmatrix} 0 & 1 \\ w_1 + 2w_2\psi & 0 \end{vmatrix} = -w_1 - 2w_2\psi.$$

Therefore, with regard to $J(\psi, \Omega) < 0$, the pair (ψ, Ω) can be designated as the saddle point. Additionally, it would be a cuspidal for

$$J(\psi, \Omega) = 0$$

and the center for $J(\psi, \Omega) > 0$. By altering the parameter ranges, the intended outcomes can be obtained.

5.3. Phase portraits under parameter variations

Case 1. $w_1 > 0, w_2 > 0$.
For the system (5.1), represented as

$$\mathcal{G}_1 = (0, 0) \quad \text{and} \quad \mathcal{G}_2 = (-1, 0)$$

as indicated in Figure 3a, we have successfully identified two stable points of equilibrium using the values $w_1 = 1$ and $w_2 = 1$. Both the center point characteristic of $\mathcal{G}_2$ and the saddle point characteristic of $\mathcal{G}_1$ are readily apparent.

Case 2. $w_1 > 0, w_2 < 0$.
The system (5.1) has two critical points for values of $w_1 = 1$ and $w_2 = -1$, namely

$$\mathcal{G}_1 = (0, 0) \quad \text{and} \quad \mathcal{G}_2 = (1, 0)$$

as shown in Figure 3b. When we look more closely, we can see that $\mathcal{G}_1$ is a saddle point, and $\mathcal{G}_2$ is the center.

Case 3. $w_1 < 0, w_2 < 0$.
We have successfully extracted the equilibrium points

$$\mathcal{G}_1 = (0, 0) \quad \text{and} \quad \mathcal{G}_2 = (-1, 0)$$

from the system (5.1) shown in Figure 3c by using the values $w_1 = -1$ and $w_2 = -1$. It is clear by looking at the phase portrait that $\mathcal{G}_1$ behaves as a center point, and $\mathcal{G}_2$ takes on the traits of a saddle.

Case 4. $w_1 < 0, w_2 > 0$.
The system (5.1) shows two equilibrium points for the values $w_1 = -1$ and $w_2 = 1$, namely

$$\mathcal{G}_1 = (0, 0) \quad \text{and} \quad \mathcal{G}_2 = (1, 0)$$

as shown in Figure 3d. $\mathcal{G}_1$ is clearly a center point, and $\mathcal{G}_2$ is clearly the saddle.

Case 5. $w_1 = 0, w_2 \neq 0$.

Only a single point of equilibrium,

$$\mathcal{G}_1 = (0, 0)$$

can be discovered for $w_1 = 0$ and $w_2 = -1$, as shown in the example in Figure 3e. By analyzing the Jacobian, it has been established that $\mathcal{G}_1$ behaves in a cusp manner.

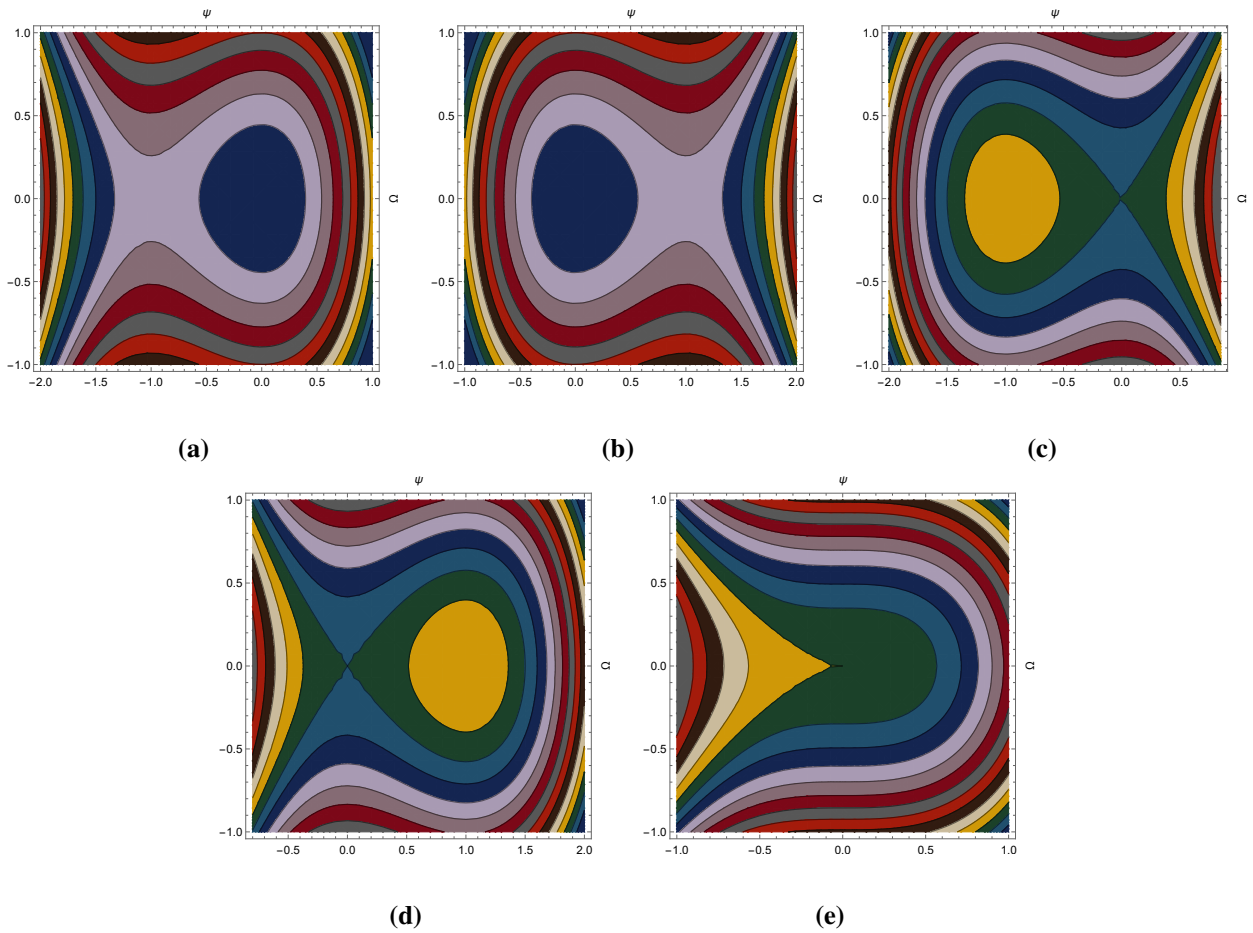

Figure 3. Dynamical analysis of the system (5.1) using the values (a) $a = \sqrt{3}$, $b = 1$, $c = 1$, $d = \sqrt{3}$, $\lambda_1 = 1$, $\lambda_2 = \frac{1}{\sqrt{3}}$, $\lambda_3 = \frac{1}{\sqrt{3}}$, $\alpha = 1$, and $w_1 = 1$, $w_2 = 1$; (b) $a = i\sqrt{3}$, $b = 1$, $c = 1$, $d = -3i\sqrt{3}$, $\lambda_1 = 1$, $\lambda_2 = \frac{1}{i\sqrt{3}}$, $\lambda_3 = \frac{1}{i\sqrt{3}}$, $\alpha = 1$, and $w_1 = 1$, $w_2 = -1$; (c) $a = i\sqrt{3}$, $b = 1$, $c = 1$, $d = 3i\sqrt{3}$, $\lambda_1 = 1$, $\lambda_2 = \frac{1}{i\sqrt{3}}$, $\lambda_3 = \frac{1}{i\sqrt{3}}$, $\alpha = 1$, and $w_1 = -1$, $w_2 = -1$; (d) $a = \sqrt{3}$, $b = 1$, $c = 1$, $d = -\frac{5}{\sqrt{3}}$, $\lambda_1 = -1$, $\lambda_2 = -\frac{1}{i\sqrt{3}}$, $\lambda_3 = -\frac{1}{i\sqrt{3}}$, $\alpha = 1$, and $w_1 = -1$, $w_2 = 1$; (e) $a = \sqrt{3}$, $b = 1$, $c = 1$, $d = -\frac{2}{\sqrt{3}}$, $\lambda_1 = -\frac{1}{3}$, $\lambda_2 = \frac{1}{\sqrt{3}}$, $\lambda_3 = \frac{1}{\sqrt{3}}$, $\alpha = 1$, and $w_1 = 0$, $w_2 = 1$.

The phase portrait analysis reveals how the system's fixed points and stability evolve with changing parameters. To explore the system's response to external periodic perturbations, we now extend our analysis to include chaotic dynamics and sensitivity studies.

6. Chaotic dynamics and sensitivity analysis

To investigate more complex dynamical behavior, we introduce a periodic perturbation to the reduced system. This enables the exploration of transitions from regular motion to chaos.

6.1. Perturbed dynamical system model

Using the previously mentioned planar dynamical system in Eq (5.1), we add the perturbation term $\zeta\cos(R)$ to investigate the disordered resolution of Eq (3.1). Thus, we obtain

$$\begin{cases} \dfrac{d\psi}{d\xi} = \Omega, \\ \dfrac{d\Omega}{d\xi} = w_1\psi + w_2\psi^2 + \zeta\cos(R), \\ \dfrac{dR}{d\xi} = \delta, \end{cases} \tag{6.1}$$

where

$$R = \delta\xi.$$

The amplitude and frequency of the external force applied to the system (6.1) are represented by the parameters ζ and δ in the given system. In the present work, we investigate the effect of the perturbation parameters $\zeta\cos(R)$ on the perturbed dynamical system (6.1). The influence of outside factors may lead a system to act randomly and unpredictably. We found this specific phenomenon in system (6.1), which is chaotic in movement in our work, whose trajectories change over time and exhibit divergences from regular patterns.

There are other methods for detecting chaos; however, in this paper, we will focus on the most useful ones:

- Bifurcation diagrams
- Sensitivity to frequency and amplitude
- Phase portraits
- Poincaré map
- Time series

6.2. Bifurcation diagrams

The theory of bifurcation has been central to the theory of nonlinear dynamic systems to describe various qualitative changes in system behavior with respect to parameter classes. When an infinitesimal and smooth change in parameter values leads to an abrupt change in the long-term dynamics of the system, that is, the transition from a stable fixed point to a periodic orbit or even to chaos from periodicity, one refers to this as a bifurcation. The bifurcation study serves to identify stability or bifurcation phenomena, transitions, and possible behavior of chaos in physical applications. By identifying bifurcation points and investigating corresponding system responses, one

can easily identify regions of both steady and unsteady motion and give physical interpretations to system parameters in terms of global dynamic behavior.

Figure 4 presents a bifurcation arrangement that corresponds to the perturbed dynamical system given by (6.1). The bifurcation diagram presents the evolution of states of the system, characterized by the state variable Ω, which varies with the bifurcation parameter ξ. The bifurcation diagram changes its character from a single-valued smooth curve to a scattered set of points, as ξ is increased.

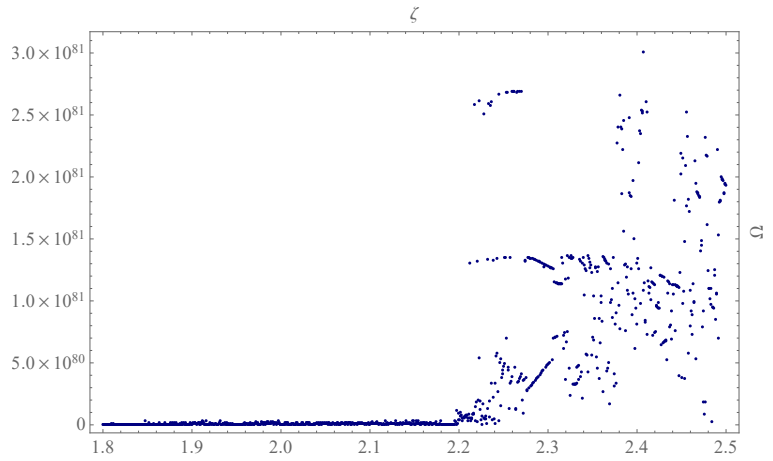

Figure 4. The bifurcation chaotic behavior of the perturbed dynamical system (CBPDS) (6.1) using the values $a = \sqrt{2}$, $b = 1$, $c = 1$, $d = -\frac{7}{\sqrt{2}}$, $\lambda_1 = -1$, $\lambda_2 = -\frac{1}{\sqrt{2}}$, $\lambda_3 = -\frac{1}{\sqrt{2}}$, $\alpha = 1$, $w_1 = -2.5$, $w_2 = 1.5$, $\delta = 1.15$ with the initial condition $(\psi(0), \Omega(0)) = (0.9, 0.5)$.

6.3. Sensitivity to frequency and amplitude

Sensitivity analysis is a significant technique for evaluating the effect of variations in external parameters on the dynamics of a nonlinear dynamical system. In chaotic systems, slight perturbations in input parameters, such as forcing frequency or amplitude, can lead to appreciable divergences of paths in the system. This phenomenon is generally known as sensitive dependence on initial conditions and parameters and represents one of the main features of chaotic dynamics. One may find thresholds beyond which the system transitions from regular, periodic motion to complex, chaotic motion via sensitivity analysis.

Figures 5 and 6 provide a clear indication of the system's sensitivity to the perturbation parameters of the external perturbations-frequency δ and amplitude ζ, respectively-of the CBPDS model. In Figure 5, the amplitude of forcing is fixed, whereas δ is varied. As the frequency increases from

$$\delta = 3.20$$

toward

$$\delta = 4.00,$$

the trace of Ω evolves from smooth oscillations into more erratic fluctuations, showing the destabilizing effect of increasing-frequency input and the initiation of chaotic motion.

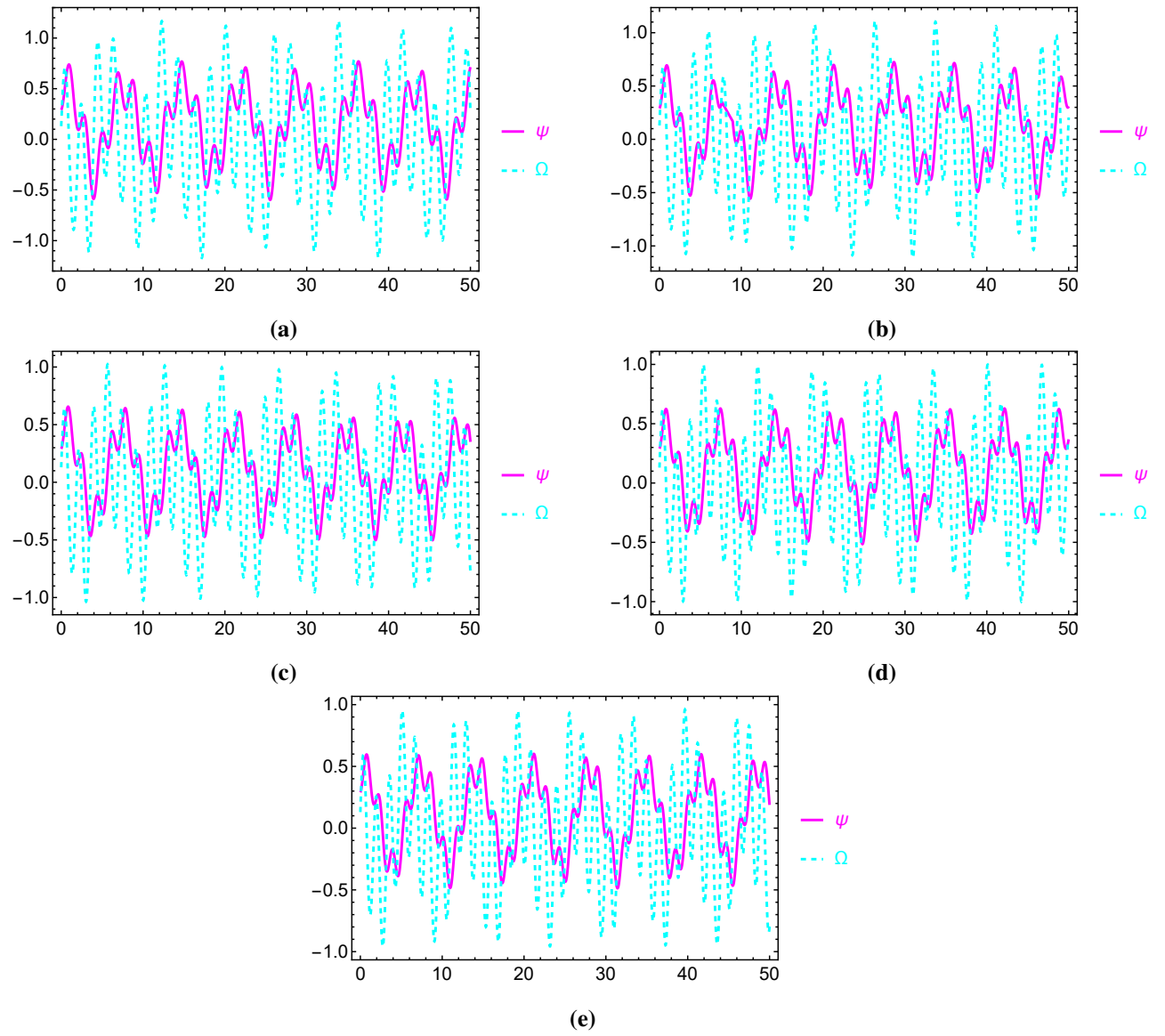

Figure 5. The sensitivity of the CBPDS (6.1) using the values $a = \sqrt{3}$, $b = 1$, $c = 1$, $d = -\frac{5}{\sqrt{3}}$, $\lambda_1 = -1$, $\lambda_2 = -\frac{1}{\sqrt{3}}$, $\lambda_3 = -\frac{1}{\sqrt{3}}$, $\delta = 1$, $w_1 = -1$, $w_2 = 1$, $\zeta = 2.20$, and (a) $\delta = 3.20$; (b) $\delta = 3.40$; (c) $\delta = 3.60$; (d) $\delta = 3.80$; (e) $\delta = 4.00$ with the initial condition $(\psi(0), \Omega(0)) = (0.29, 0.13)$.

Conversely, in Figure 6, δ is held fixed at 4.00, and ζ is increased from 2.20 to 3.00. The corresponding time series reveal that as ζ grows, the system exhibits larger nonlinear response, with oscillations more random and less predictable. This reveals that the larger external excitation drives the system towards a chaotic state. Collectively, these figures support the dual function of frequency and amplitude in system stability control and describe how well-balanced external parameters can induce enormous effects on dynamic behavior.

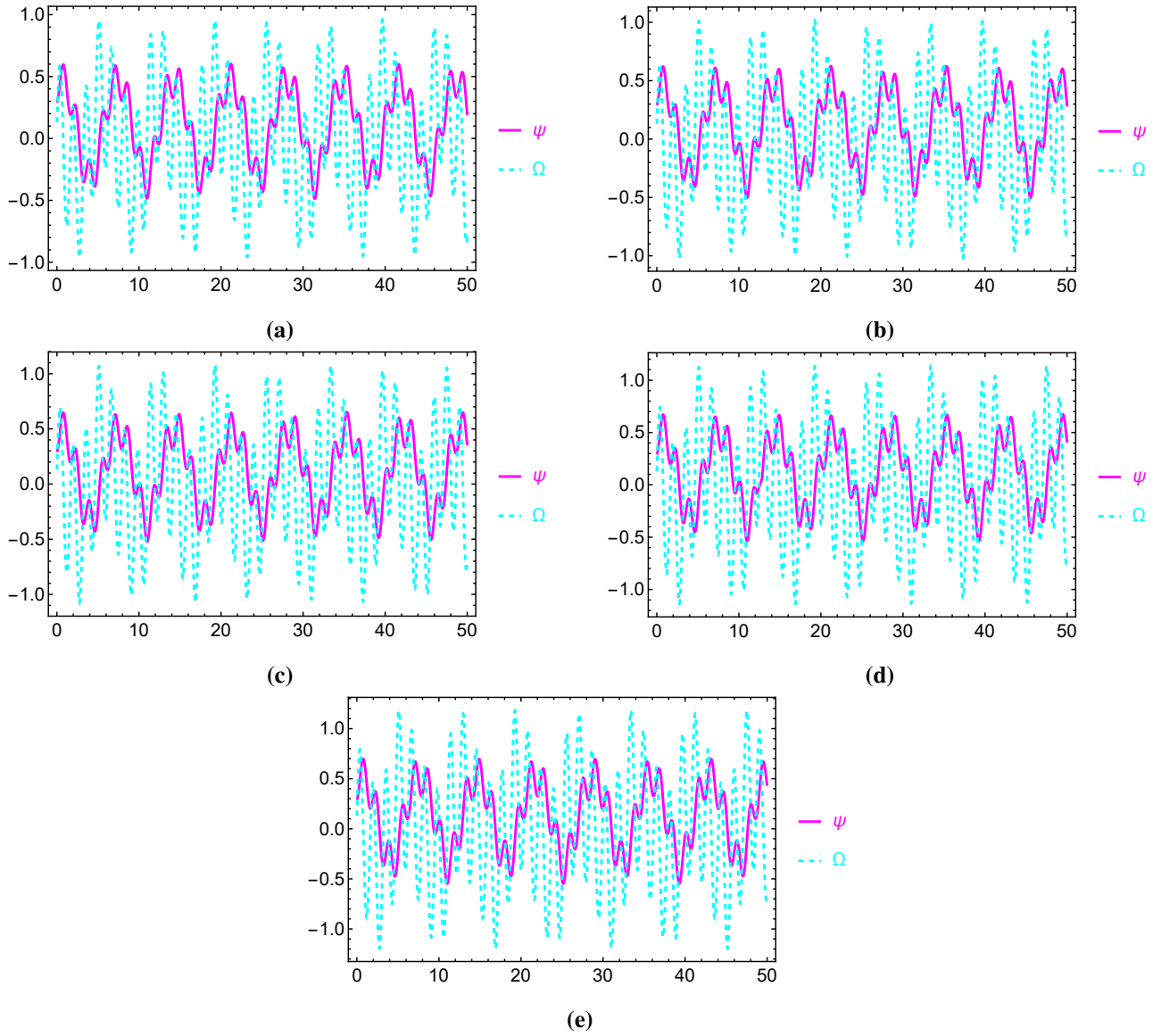

Figure 6. The sensitivity of the CBPDS (6.1) using the values $a = \sqrt{3}$, $b = 1$, $c = 1$, $d = -\frac{5}{\sqrt{3}}$, $\lambda_1 = -1$, $\lambda_2 = -\frac{1}{\sqrt{3}}$, $\lambda_3 = -\frac{1}{\sqrt{3}}$, $\alpha = 1$, $w_1 = -1$, $w_2 = 1$, $\delta = 4.00$, and (a) $\zeta = 2.20$; (b) $\zeta = 2.40$; (c) $\zeta = 2.60$; (d) $\zeta = 2.80$; (e) $\zeta = 3.00$ with the initial condition $(\psi(0), \Omega(0)) = (0.29, 0.13)$.

6.4. Phase portraits (2D and 3D)

Phase portraits are powerful geometric means of expressing state space structure and stability properties of dynamic systems. By plotting the trajectories in the (ψ, Ω) or (ψ, Ω, R) planes, one can immediately observe features such as attractors, limit cycles, saddle points, and chaotic orbits. Phase portraits are especially helpful in differentiating regular (e.g., periodic or quasi-periodic) versus chaotic dynamics by organization, density, and divergence of trajectories.

Figures 7 and 8 are the 2D phase portraits of the CBPDS model for varying forcing frequency δ

and amplitude ζ, respectively. In Figure 7, the phase curves are distorted and broken up as δ increases, exhibiting a clear onset of periodic to chaotic behavior.

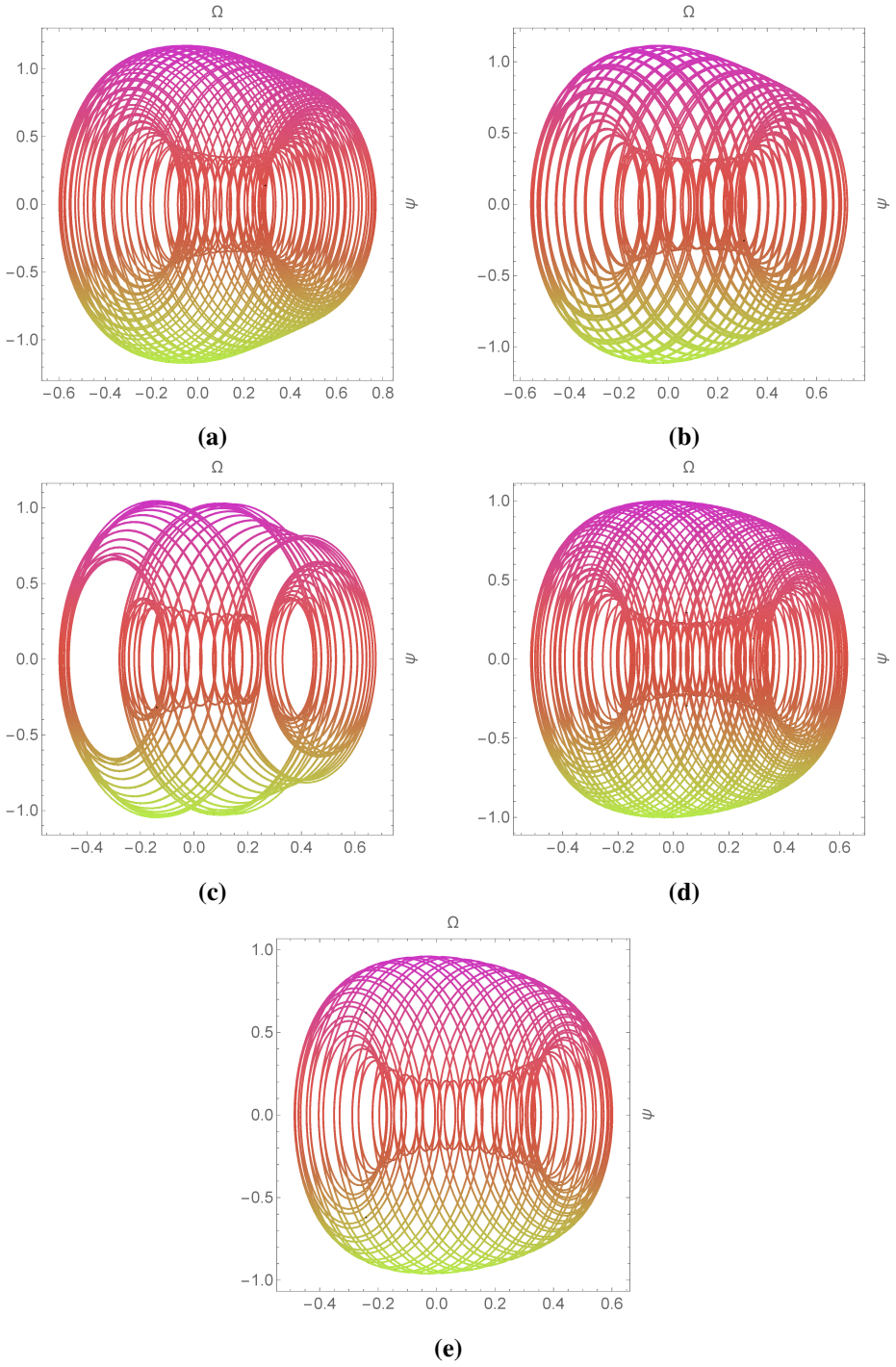

Figure 7. 2D phase portrait of the CBPDS (6.1) using the values $a = \sqrt{3}$, $b = 1$, $c = 1$, $d = -\frac{5}{\sqrt{3}}$, $\lambda_1 = -1$, $\lambda_2 = -\frac{1}{\sqrt{3}}$, $\lambda_3 = -\frac{1}{\sqrt{3}}$, $\alpha = 1$, $w_1 = -1$, $w_2 = 1$, $\zeta = 2.20$, and (a) $\delta = 3.20$; (b) $\delta = 3.40$; (c) $\delta = 3.60$; (d) $\delta = 3.80$; (e) $\delta = 4.00$ with the initial condition $(\psi(0), \Omega(0)) = (0.29, 0.13)$.

Similarly, Figure 8 demonstrates how an increase in amplitude ζ produces more scattered and unpredictable trajectories, establishing the system's growing sensitivity toward the amplitude of external excitation.

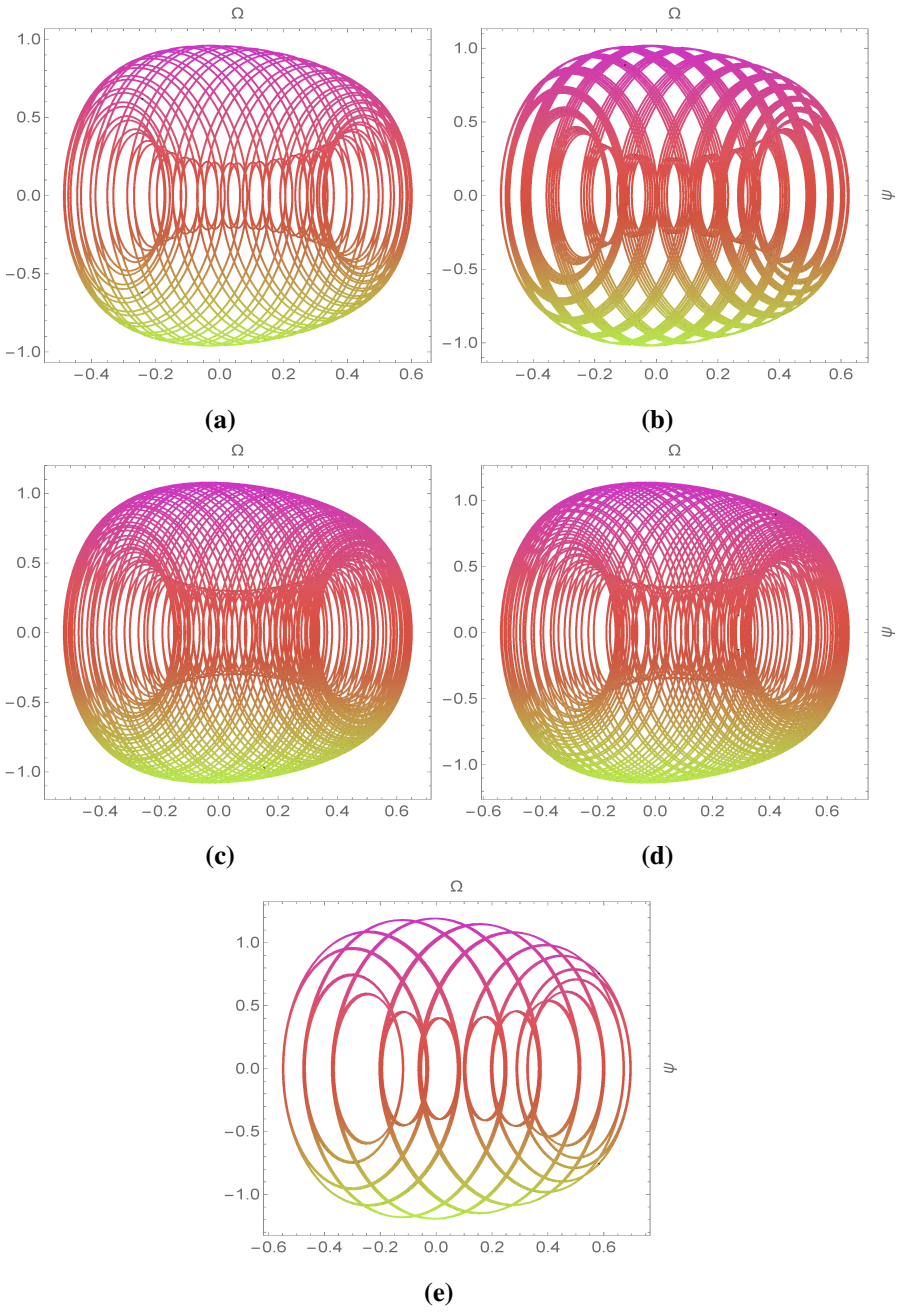

Figure 8. 2D phase portrait of the CBPDS (6.1) using the values $a = \sqrt{3}$, $b = 1$, $c = 1$, $d = -\frac{5}{\sqrt{3}}$, $\lambda_1 = -1$, $\lambda_2 = -\frac{1}{\sqrt{3}}$, $\lambda_3 = -\frac{1}{\sqrt{3}}$, $\alpha = 1$, $w_1 = -1$, $w_2 = 1$, $\delta = 4.00$, and (a) $\zeta = 2.20$; (b) $\zeta = 2.40$; (c) $\zeta = 2.60$; (d) $\zeta = 2.80$; (e) $\zeta = 3.00$ with the initial condition $(\psi(0), \Omega(0)) = (0.29, 0.13)$.

Figures 9 and 10 give the 3D phase portraits for the corresponding parameter changes. The three-

dimensional perspectives show tangled spiral structures and knotted orbits that are typical of chaotic attractors. As δ or ζ increases, orbits lose coherence and begin to cover larger areas of the phase space in a non-periodic pattern. These observations confirm the emergence of chaos and show the richness of the underlying dynamic behavior in the perturbed Boussinesq-type model.

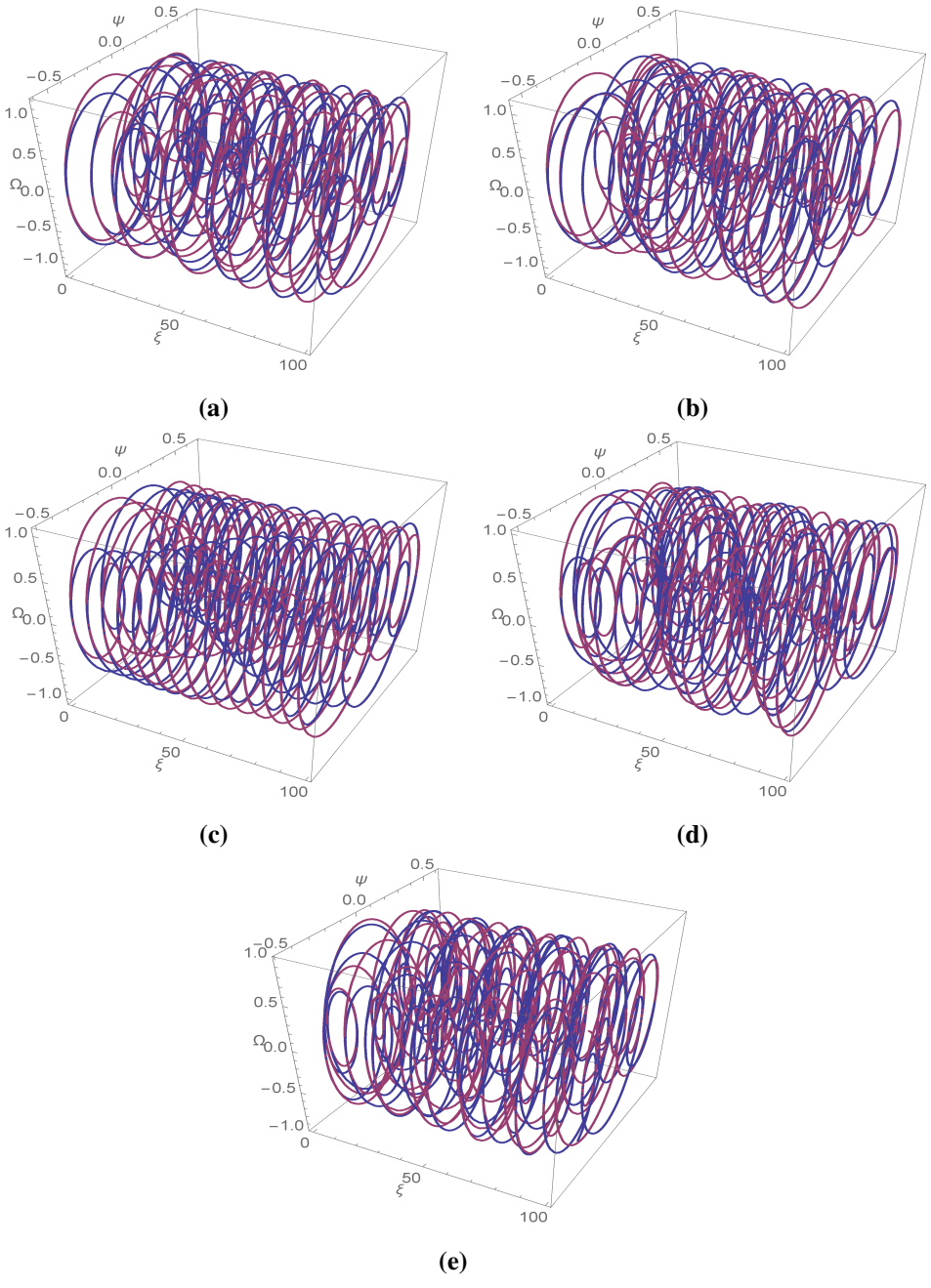

Figure 9. 3D phase portrait of the CBPDS (6.1) using the values $a = \sqrt{3}$, $b = 1$, $c = 1$, $d = -\frac{5}{\sqrt{3}}$, $\lambda_1 = -1$, $\lambda_2 = -\frac{1}{\sqrt{3}}$, $\lambda_3 = -\frac{1}{\sqrt{3}}$, $\alpha = 1$, $w_1 = -1$, $w_2 = 1$, $\zeta = 2.20$, and (a) $\delta = 3.20$; (b) $\delta = 3.40$; (c) $\delta = 3.60$; (d) $\delta = 3.80$; (e) $\delta = 4.00$ with the initial condition $(\psi(0), \Omega(0)) = (0.29, 0.13)$.

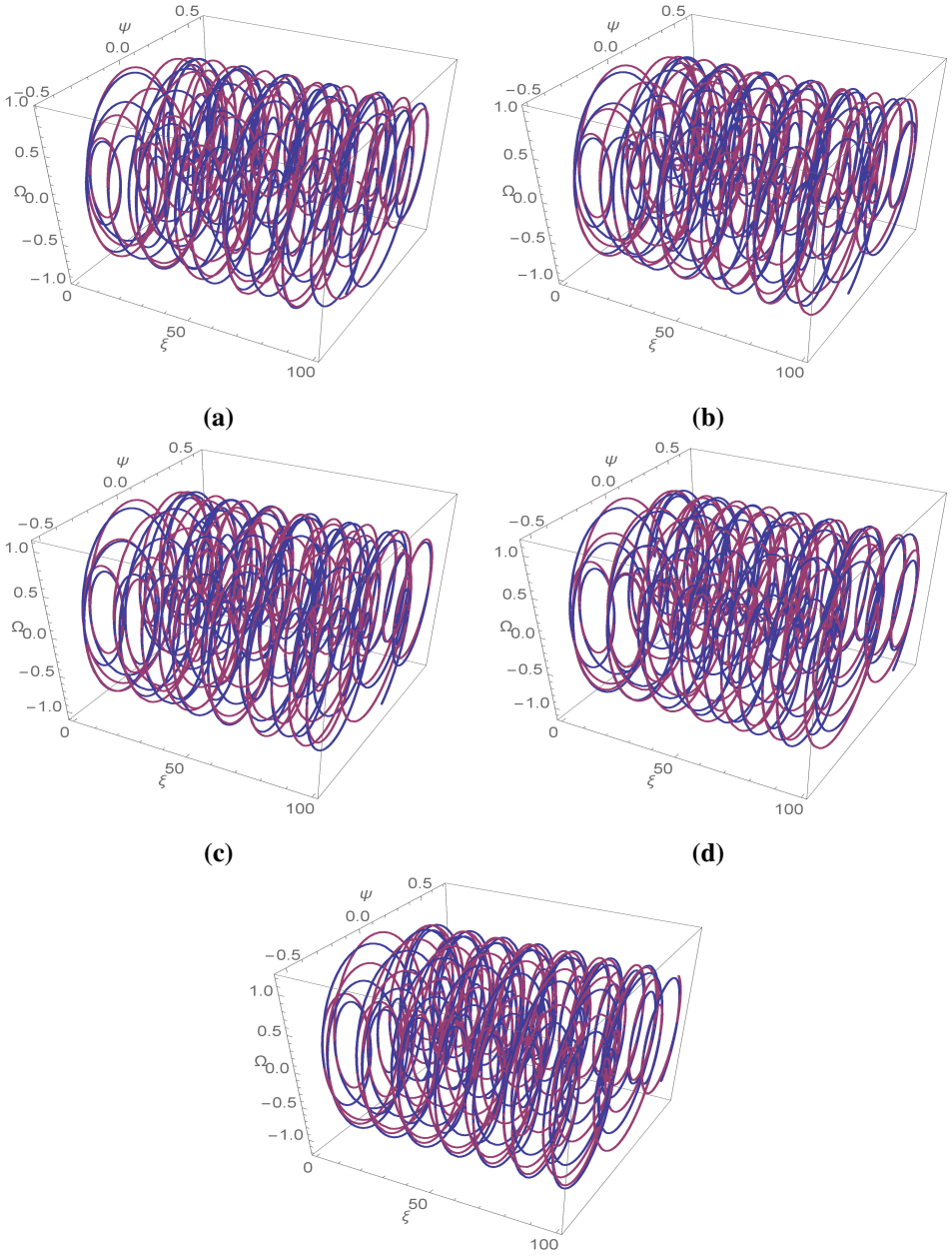

Figure 10. 3D phase portrait of the CBPDS (6.1) using the values $a = \sqrt{3}$, $b = 1$, $c = 1$, $d = -\frac{5}{\sqrt{3}}$, $\lambda_1 = -1$, $\lambda_2 = -\frac{1}{\sqrt{3}}$, $\lambda_3 = -\frac{1}{\sqrt{3}}$, $\alpha = 1$, $w_1 = -1$, $w_2 = 1$, $\delta = 4.00$, and (a) $\zeta = 2.20$; (b) $\zeta = 2.40$; (c) $\zeta = 2.60$; (d) $\zeta = 2.80$; (e) $\zeta = 3.00$ with the initial condition $(\psi(0), \Omega(0)) = (0.29, 0.13)$.

6.5. Poincaré map

The Poincaré map is a well-known diagnostic technique used to detect and describe chaotic behavior in nonlinear systems. By sampling the system at discrete phase or time, the Poincaré section translates

a continuous dynamical system into a discrete map, providing information on attractor structure. For regular or periodic regimes, the Poincaré map provides a collection of finite numbers of points or closed orbits. Chaotic systems, on the other hand, produce filled or densely scattered patterns, which implies sensitivity to initial conditions and the breakdown of periodic motion.

Figure 11 presents the Poincaré maps of the CBPDS model for different values of forcing frequency δ with ζ fixed. The transition from ordered points toward increasingly irregular scatterings confirms the destabilizing effect of higher-frequency perturbations.

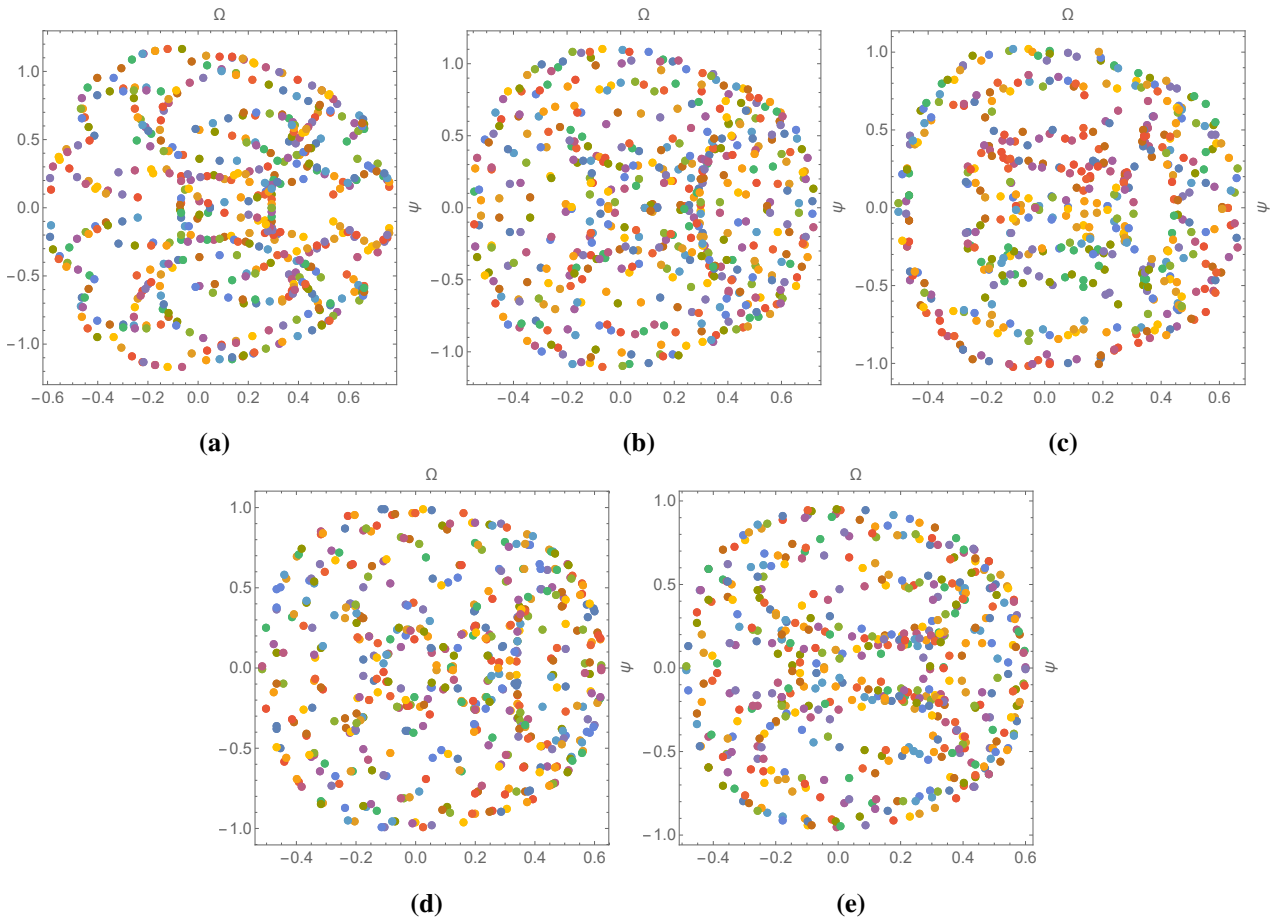

Figure 11. Poincaré map of the CBPDS (6.1) using the values $a = \sqrt{3}$, $b = 1$, $c = 1$, $d = -\frac{5}{\sqrt{3}}$, $\lambda_1 = -1$, $\lambda_2 = -\frac{1}{\sqrt{3}}$, $\lambda_3 = -\frac{1}{\sqrt{3}}$, $\alpha = 1$, $w_1 = -1$, $w_2 = 1$, $\zeta = 2.20$, and (a) $\delta = 3.20$; (b) $\delta = 3.40$; (c) $\delta = 3.60$; (d) $\delta = 3.80$; (e) $\delta = 4.00$ with the initial condition $(\psi(0), \Omega(0)) = (0.29, 0.13)$.

Analogously, Figure 12 shows the maps of various amplitude ζ with fixed frequency $\delta = 4.00$. As ζ increases, isolated points in the Poincaré section fan out into more complex and seemingly random patterns. The regimes provide substantial evidence of chaotic attractors governing the system's dynamics and suggest how both δ and ζ are accountable for inducing chaos in the perturbed dynamical system model.

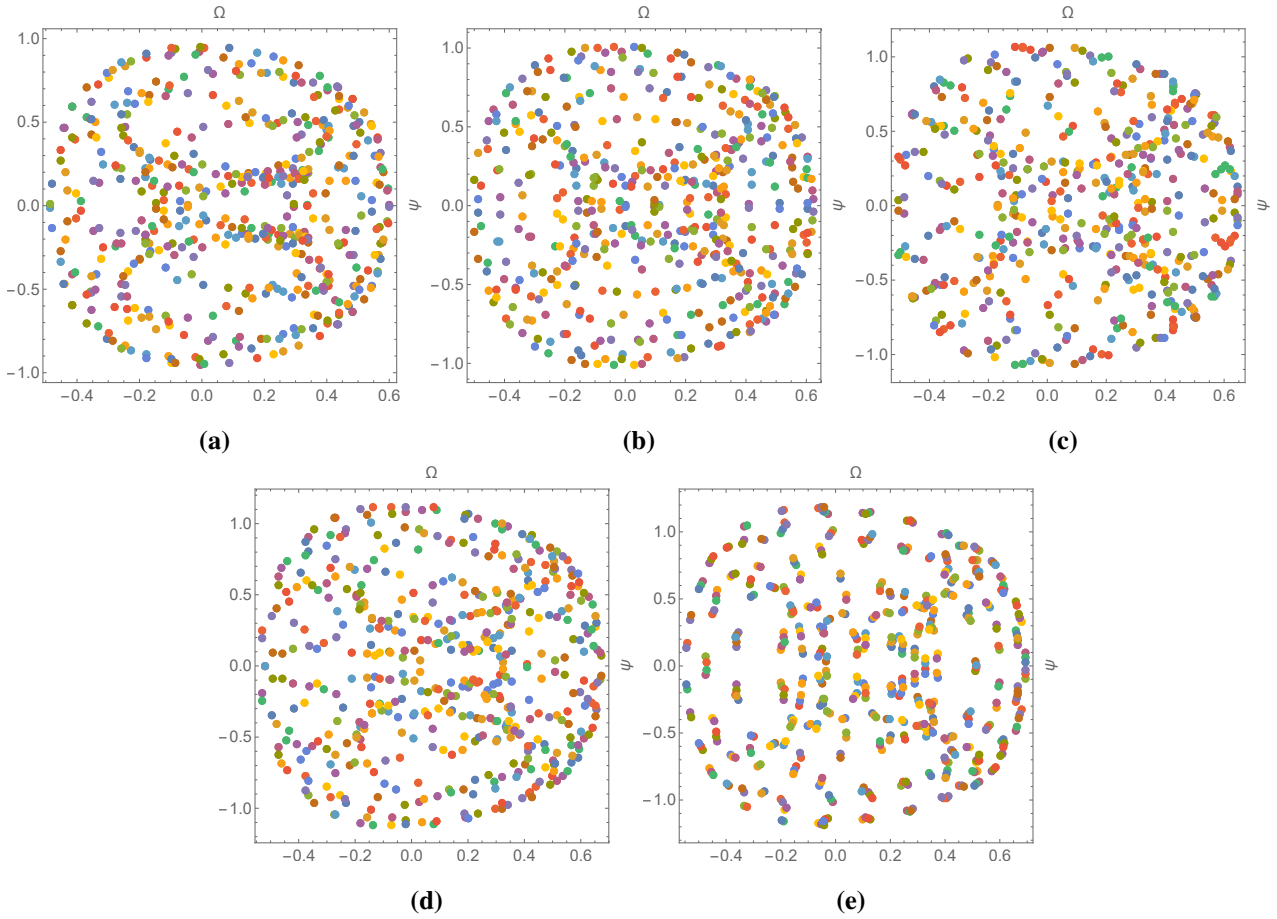

Figure 12. Poincaré map of the CBPDS (6.1) using the values $a = \sqrt{3}$, $b = 1$, $c = 1$, $d = -\frac{5}{\sqrt{3}}$, $\lambda_1 = -1$, $\lambda_2 = -\frac{1}{\sqrt{3}}$, $\lambda_3 = -\frac{1}{\sqrt{3}}$, $\alpha = 1$, $w_1 = -1$, $w_2 = 1$, $\delta = 4.00$, and (a) $\zeta = 2.20$; (b) $\zeta = 2.40$; (c) $\zeta = 2.60$; (d) $\zeta = 2.80$; (e) $\zeta = 3.00$ with the initial condition $(\psi(0), \Omega(0)) = (0.29, 0.13)$.

6.6. Time series

Time series analysis is a simple approach to examining the time evolution of dynamical systems. By tracking the stationary behavior of a system variable over time, evidence for regular oscillations, transients, or apparently random chaotic fluctuations may be discovered. Time series in chaotic systems are usually found to exhibit aperiodicity, amplitude modulation, and sensitive initial-condition dependence-key features of deterministic chaos.

Figure 13 depicts the time series of state variable Ω for progressively higher values of forcing frequency δ, but with fixed amplitude ζ. When δ takes low values, the system is defined by well-smoothed, periodic oscillations. For progressively higher values of δ, however, the waveforms become progressively more random in nature, displaying nonsmooth peaks and intervals, suggesting the emergence of chaos via frequency-induced bifurcations.

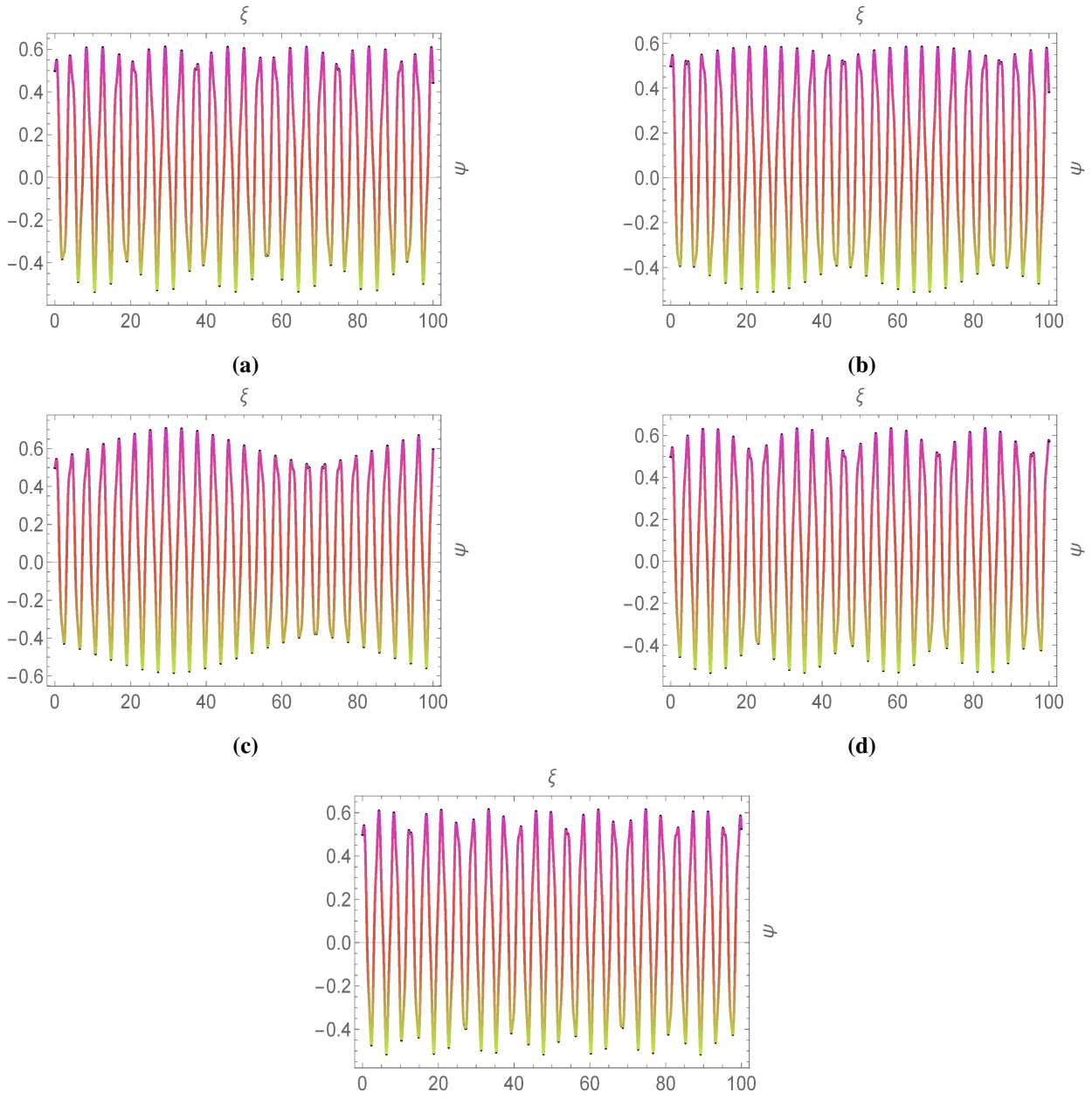

Figure 13. Time series of the CBPDS (6.1) using the values $a = \sqrt{2}$, $b = 1$, $c = 1$, $d = -\frac{7}{\sqrt{2}}$, $\lambda_1 = -1$, $\lambda_2 = -\frac{1}{\sqrt{2}}$, $\lambda_3 = -\frac{1}{\sqrt{2}}$, $\alpha = 1$, $w_1 = -2.5$, $w_2 = 1.5$, $\zeta = 1.25$, and (a) $\delta = 4.20$; (b) $\delta = 4.40$; (c) $\delta = 4.60$; (d) $\delta = 4.80$; (e) $\delta = 5.00$ with the initial condition $(\psi(0), \Omega(0)) = (0.5, 0.1)$.

Also illustrated in Figure 14 is the system response with growing ζ for fixed δ. The waveforms become increasingly random patterns as the forcing amplitude grows. These results validate that external disturbance frequency and amplitude are critical factors in determining the dynamical regime of the system, and that chaotic behavior can be robustly induced by controlled parameter modulation.

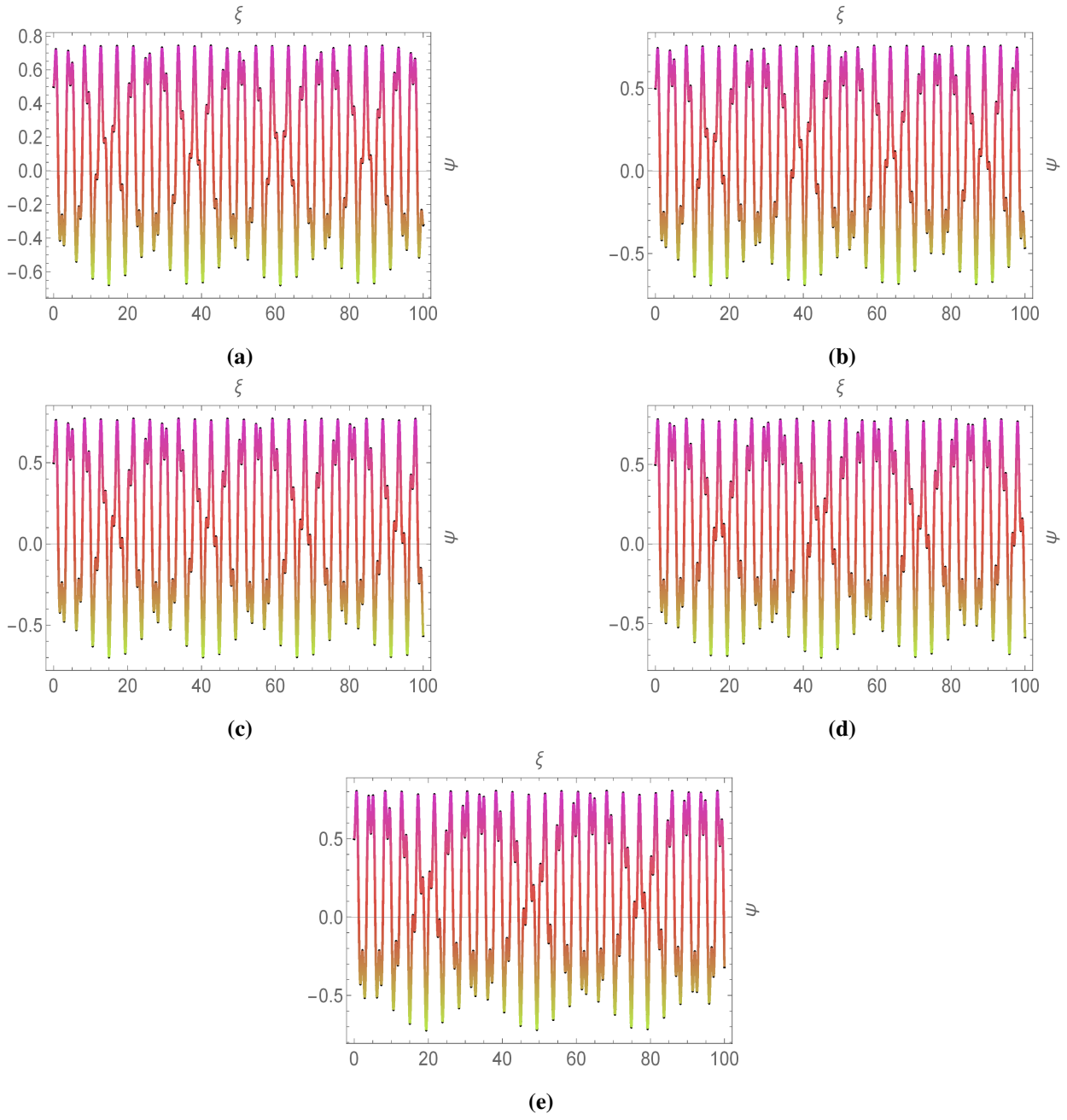

Figure 14. Time series of the CBPDS (6.1) using the values $a = \sqrt{2}$, $b = 1$, $c = 1$, $d = -\frac{7}{\sqrt{2}}$, $\lambda_1 = -1$, $\lambda_2 = -\frac{1}{\sqrt{2}}$, $\lambda_3 = -\frac{1}{\sqrt{2}}$, $\alpha = 1$, $w_1 = -2.5$, $w_2 = 1.5$, $\delta = 4.20$, and (a) $\zeta = 3.20$; (b) $\zeta = 3.40$; (c) $\zeta = 3.60$; (d) $\zeta = 3.80$; (e) $\zeta = 4.00$ with the initial condition $(\psi(0), \Omega(0)) = (0.5, 0.1)$.

7. Numerical simulations

This section summarizes the numerical observations obtained for the perturbed system and demonstrates how the numerical behavior supports and extends the analytical findings.

To complement the analytical and qualitative analysis, numerical simulations were carried out to explore the dynamical behavior of the CBPDS model under various parameter configurations. These simulations help validate the theoretical predictions and provide concrete illustrations of how the system responds to changes in its governing parameters.

Figure 1 shows a stable localized soliton for $\lambda^2 - 4\eta > 0$, $\eta \neq 0$, with amplitude and width preserved during propagation. Figure 2 illustrates a periodic-type oscillatory wave train for $\lambda^2 - 4\eta < 0$, $\eta \neq 0$, where repeating crests and troughs remain stable over time. Figure 3 demonstrates the phase portraits of the reduced system under five distinct cases for combinations of w_1 and w_2, showing center, saddle, and cusp-type behaviors that reflect the local stability of equilibrium points. The bifurcation structure is further examined in Figure 4, where the chaotic transitions are captured by tracking Ω over a range of the bifurcation parameter ζ. Figures 5 and 6 present sensitivity plots with respect to frequency δ and amplitude ζ, respectively, confirming the system's responsiveness to external periodic forcing. In Figures 7–10, 2D and 3D phase portraits reveal the evolution from periodic orbits to chaotic attractors under increasing perturbations. Poincaré sections in Figures 11 and 12 depict the transformation of phase space from discrete points to densely scattered sets, indicating chaotic dynamics. Finally, the time series shown in Figures 13 and 14 illustrate the progression from smooth oscillations to irregular and unpredictable temporal patterns.

These comprehensive simulations reinforce the theoretical findings and confirm the rich dynamical structure of the model, highlighting transitions among stable, bifurcating, and chaotic regimes across different parameter regimes.

Remark. Some parameters listed in this section, such as $a = i\sqrt{3}$, originate from the analytical solution construction in Section 3. These complex-valued constants are intermediate algebraic parameters that arise from the auxiliary equation used in the $\exp(-\varphi(\xi))$-expansion method. They are not used in the real-valued dynamical system analyzed in Sections 5 and 6, nor do they play any role in the phase portraits or numerical simulations. All dynamical analysis are performed entirely with real-valued parameters.

8. Conclusions

In this study, we examined the analytical and dynamical properties of a (3+1)-dimensional 1eKP equation that incorporates higher-order nonlinear and dispersive effects. By utilizing the $\exp(-\varphi(\xi))$-expansion method, we successfully obtained exact traveling wave solutions in closed form. The derived solutions include localized solitary waves, breathing structures, and periodic profiles, which highlight the diverse and complex behavior supported by the underlying equation. To further analyze the system, a reduction via traveling wave transformation led to a planar dynamical system. A detailed bifurcation analysis was performed, classifying equilibrium points and their stability characteristics based on parameter variations. The phase portraits illustrated rich topological structures, including centers, saddles, and cusp points, which signal critical transitions in the system's dynamics. To investigate the influence of external excitation, a periodic forcing term was introduced, leading to a perturbed dynamical system. The presence of chaotic dynamics was confirmed through bifurcation diagrams, sensitivity analysis, phase portraits (2D and 3D), Poincaré sections, and time series plots. These tools revealed how the system responds to changes in forcing frequency and amplitude, with clear transitions from regular oscillatory motion to irregular and chaotic behavior.

Numerical simulations were carried out to validate and visualize the theoretical results, showing consistency across all analytical and qualitative analysis. The outcomes demonstrate the capacity of the proposed model to capture complex wave dynamics, offering valuable insights into nonlinear wave propagation in multidimensional settings. Future work could extend the analysis to consider damping effects, multi-soliton interactions, or more general classes of external perturbations. Additionally, hybrid numerical-analytical techniques or data-driven models such as neural network-based solvers could be employed to explore solution landscapes beyond the reach of classical methods.

Author contributions

Bahadır Kopçasız: software; visualization; writing-original draft; methodology; validation; conceptualization; Rubayyi T. Alqahtani: software; visualization; writing-original draft; methodology; validation; conceptualization; Mehmet Şenol: software; visualization; writing-original draft; methodology; validation; conceptualization. All authors have read and approved the final version of the manuscript for publication.

Use of Generative-AI tools declaration

The authors declare they have not used artificial intelligence (AI) tools in the creation of this article.

Fundings

This work was supported and funded by the Deanship of Scientific Research at Imam Mohammad Ibn Saud Islamic University (IMSIU) (grant number IMSIU-DDRSP2602).

Conflict of interest

The authors declare that they have no conflicts of interest.

References

1. L. Akinyemi, Solutions of generalized fractional perturbed Zakharov-Kuznetsov equation arising in a magnetized dusty plasma, *Rev. Mex. Fís.*, **67** (2021), 060703. https://doi.org/10.31349/revmexfis.67.060703
2. L. Akinyemi, I. Ainomugisha, Stability and solitary wave dynamics of higher-dimensional nonlinear Schrödinger equation with time-dependent potential, *Nonlinear Dyn.*, **113** (2025), 23439–23456. https://doi.org/10.1007/s11071-025-11325-7
3. S. Kumar, A. Kukkar, Dynamics of several optical soliton solutions of a (3+1)-dimensional nonlinear Schrödinger equation with parabolic law in optical fibers, *Mod. Phys. Lett. B*, **39** (2024), 2450453. https://doi.org/10.1142/S0217984924504530
4. M. Ozisik, S. A. Durmus, A. Secer, M. Bayram, Pure-cubic optical soliton solutions of the nonlinear Schrödinger equation including parabolic law nonlinearity in the absence of the group velocity dispersion, *Int. J. Theor. Phys.*, **64** (2025), 80. https://doi.org/10.1007/s10773-025-05950-6

5. Z. Yang, W. P. Zhong, M. Belić, Dark localized waves in shallow waters: analysis within an extended Boussinesq system, *Chin. Phys. Lett.*, **41** (2024), 044201. https://doi.org/10.1088/0256-307X/41/4/044201
6. K. J. Wang, X. L. Liu, F. Shi, G. Li, Bifurcation and sensitivity analysis, chaotic behaviors, variational principle, Hamiltonian and diverse wave solutions of the new extended integrable Kadomtsev–Petviashvili equation, *Phys. Lett. A*, **534** (2025), 130246. https://doi.org/10.1016/j.physleta.2025.130246
7. P. Xu, H. Huang, K. J. Wang, Dynamics of real and complex multi-soliton solutions, novel soliton molecules, asymmetric solitons and diverse wave solutions to the Kadomtsev-Petviashvili equation, *Alex. Eng. J.*, **125** (2025), 537–544. https://doi.org/10.1016/j.aej.2025.04.040
8. Beenish, M. Samreen, F. S. Alshammari, Exploring solitary wave solutions of the generalized integrable Kadomtsev–Petviashvili equation via Lie symmetry and Hirota's bilinear mthod, *Symmetry*, **17** (2025), 710. https://doi.org/10.3390/sym17050710
9. M. H. Rafiq, J. Lin, Periodic breather waves, stripe-solitons and interaction solutions for the (3+1)-dimensional variable-coefficient Kadomtsev–Petviashvili-like equation, *Chaos Solitons Fract.*, **194** (2025), 116212. https://doi.org/10.1016/j.chaos.2025.116212
10. M. Şenol, M. Ö. Erol, F. M. Çelik, N. Das, Dynamical investigation of the new (3+1)-dimensional Kadomtsev–Petviashvili-Sawada-Kotera-Ramani equation with conformable fractional derivative, *Mod. Phys. Lett. B*, **39** (2025), 2550110. https://doi.org/10.1142/S0217984925501106
11. I. Samir, H. M. Ahmed, H. Emadifar, K. K. Ahmed, Traveling and soliton waves and their characteristics in the extended (3+1)-dimensional Kadomtsev-Petviashvili equation in fluid, *Part. Differ. Equations Appl. Math.*, **14** (2025), 101146. https://doi.org/10.1016/j.padiff.2025.101146
12. J. G. Liu, W. H. Zhu, Y. He, Variable-coefficient symbolic computation approach for finding multiple rogue wave solutions of nonlinear system with variable coefficients, *Z. Angew. Math. Phys.*, **72** (2021), 154. https://doi.org/10.1007/s00033-021-01584-w
13. B. B. Kadomtsev, V. I. Petviashvili, On the stability of solitary waves in weakly dispersive media, *Sov. Phys. Dokl.*, **15** (1970), 539–541.
14. L. Kaur, A. M. Wazwaz, Dynamical analysis of soliton solutions for space-time fractional Calogero-Degasperis and Sharma-Tasso-Olver equations, *Rom. Rep. Phys.*, **74** (2022), 108.
15. F. Yuan, Deformed soliton and positon solutions for the (2+1)-dimensional nonlinear Schrödinger equation, *Rom. Rep. Phys.*, **74** (2022), 121.
16. A. M. Wazwaz, W. Alhejaili, S. A. El-Tantawy, New (3+1)-dimensional Painlevé integrable extensions of Mikhailov-Novikov-Wang equation: variety of multiple soliton solutions, *Rom. J. Phys.*, **67** (2022), 115.
17. M. Şenol, B. Ghanbari, Exploration of novel traveling wave solitons to the conformable (3+1)-dimensional Wazwaz-Kaur-Boussinesq equation, *Int. J. Theor. Phys.*, **64** (2025), 151. https://doi.org/10.1007/s10773-025-06018-1
18. M. Wang, G. He, T. Xu, N. Li, Localized waves for modified Boussinesq equation and Mikhailov-Lenells equation based on Physics-informed neural networks and Miura transformation, *Chaos Solitons Fract.*, **190** (2025), 115764. https://doi.org/10.1016/j.chaos.2024.115764

19. G. Chen, K. Fang, J. Sun, Z. Liu, P. Wang, H. Jin, A two-layer Boussinesq-type wave model accelerated by graphics processing unit, *Phys. Fluids*, **37** (2025), 073606. https://doi.org/10.1063/5.0268831
20. Y. Cheng, C. Dong, S. Zheng, W. Hu, Solving nonlinear Boussinesq equation of second-order time derivatives with physics-informed neural networks, *Commun. Theor. Phys.*, **77** (2025), 105001. https://doi.org/10.1088/1572-9494/adcc8e
21. Y. L. Ma, A. M. Wazwaz, B. Q. Li, New extended Kadomtsev–Petviashvili equation: multiple soliton solutions, breather, lump and interaction solutions, *Nonlinear Dyn.*, **104** (2021), 1581–1594. https://doi.org/10.1007/s11071-021-06357-8
22. Y. L. Ma, A. M. Wazwaz, B. Q. Li, Novel bifurcation solitons for an extended Kadomtsev-Petviashvili equation in fluids, *Phys. Lett. A*, **413** (2021), 127585. https://doi.org/10.1016/j.physleta.2021.127585
23. A. M. Wazwaz, Study of three integrable extensions of Kadomtsev–Petviashvili, Boussinesq, and Kadomtsev–Petviashvili–Boussinesq equations, *Rom. Rep. Phys.*, **76** (2024), 114. https://doi.org/10.59277/romrepphys.2024.76.114
24. A. M. Wazwaz, Extensions of Kadomtsev–Petviashvili and Kadomtsev–Petviashvili–Boussinesq equations: multiple solitons and lump wave solutions, *Roma. Rep. Phys.*, **77** (2025), 115.
25. N. Kadkhoda, H. Jafari, Analytical solutions of the Gerdjikov-Ivanov equation by using exp $(-\varphi(\xi))$-expansion method, *Optik*, **139** (2017), 72–76. https://doi.org/10.1016/j.ijleo.2017.03.078

AIMS Press